

A 66-Nuclear All-Alkynyl Protected Peanut-Shaped Silver(I)/Copper(I) Heterometallic Nanocluster: Intermediate in Copper-Catalyzed Alkyne-Azide Cycloaddition

Jin-Ping Gao, Fu-Qiang Zhang, and Xian-Ming Zhang*

Ligand-protected heterometallic nanoclusters in contrast to homo-metal counterparts show more broad applications due to the synergistic effect of hetero-metals but their controllable syntheses remain a challenge. Among heterometallic nanoclusters, monovalent Ag-Cu compounds are rarely explored due to much difference of Ag(I) and Cu(I) such as atom radius, coordination habits, and redox potential. Encouraged by copper-catalyzed alkyne-azide cycloaddition (CuAAC) reaction, comproportionation reaction of Cu(II)X₂ and Cu(0) in the presence of (PhC≡CAg)_n complex and molybdate generated a core-shell peanut-shaped 66-nuclear Ag(I)-Cu(I) heterometallic nanocluster, [(Mo₄O₁₆)₂@Cu₁₂Ag₅₄(PhC≡C)₅₀] (referred to as Ag₅₄Cu₁₂). The structure and composition of Ag-Cu heterometallic nanocluster are fully characterized. X-ray single crystal diffraction reveals that Ag₅₄Cu₁₂ has a peanut-shaped silver(I)/copper(I) heterometallic nanocage protected by fifty phenylacetylene ligands in μ₃-modes and encapsulated two mutually twisted tetramolybdates. Heterometallic nanocage contains a 54-Ag-atom outer ellipsoid silver cage decorated by 12 copper inside wall. Nanosized Ag₅₄Cu₁₂ is a *n*-type narrow-band-gap semiconductor with a good photocurrent response. Preliminary experiments demonstrates that Ag₅₄Cu₁₂ itself and activated carbon supported Ag₅₄Cu₁₂/C are effective catalysts for 1,3-dipole cycloaddition between alkynes and azides at ambient conditions. The work provides not only a new synthetic route toward Ag(I)-Cu(I) nanoclusters but also an important heterometallic intermediate in CuAAC catalytic reaction.

1. Introduction

High-nuclearity ligand-protected heterometallic nanoclusters are more attractive than homo-metal nanoclusters for potential applications such as catalysis, photoluminescence, electrochemistry, and other fields, which is due to the synergistic effect of hetero-metal nanoclusters on physicochemical properties.^[1] The key to tuning physicochemical behavior of heterometallic clusters is the preparation of nanoclusters with controllable composition/doping sites.^[2] Generally, heteroatoms that can be dope into silver nanoclusters are noble metals with similar radius in the periodic table.^[3] Conventional doping methods are based on co-reduction, metal exchange, metal deposition of atoms/ions [(also known as anti-galvanic reaction (AGR)), or a combination of these strategies.^[4] These strategies are less effective in controlling reduction of double metal salts and formation of heteroatomic nanoclusters. A search reveals that the availability of heteronuclear Ag(I)-Cu(I) alkynyl clusters via Cu doping are rare.^[5] As far as dopants of Cu element are concerned, the standard potential of Cu²⁺/Cu⁺ couple is as low as

159 mV, which indicates that the +1 oxidation state of copper is susceptible to be oxidized to much more stable +2 state. Furthermore, the aggregative nature of Cu(I) alkynyl causes a larger challenge in isolation of discrete Ag(I)-Cu(I) alkynyl nanoclusters. To solve this puzzle, the comproportionation reaction based copper-catalyzed alkyne-azide cycloaddition (CuAAC) reaction could provide a route toward stable homogeneous high-nuclearity monovalent copper alkynyl clusters.^[6] The origin of Cu(I) intermediate is generated by Cu(II) with various Cu(0) sources such as wire, turnings, powder and nanoparticles in CuAAC reaction. This reaction could overcome potential difference to produce monovalent copper,^[7] which in combination with a variety of alkynyl precursors give metal nanoclusters with tunable composition, structure, and properties.^[8] In spite of success in homogeneous copper, the implementation of the experiments remains a challenge in heterogeneous Cu/Ag nanoclusters(.

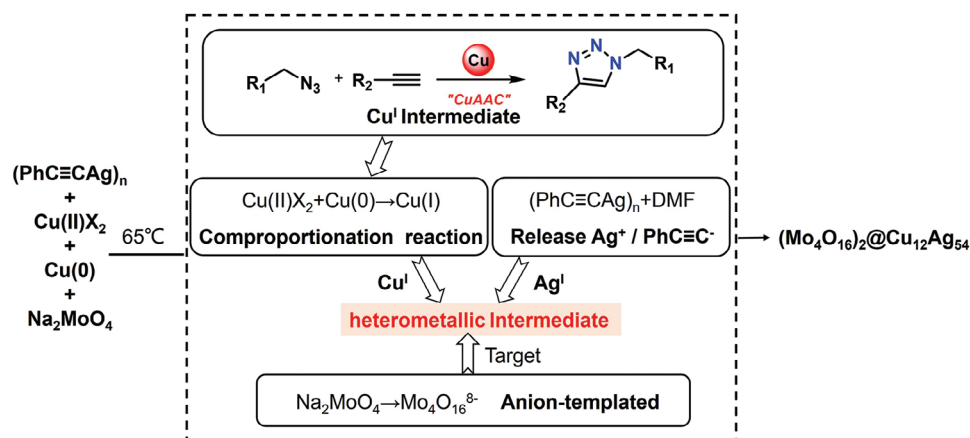
J.-P. Gao, F.-Q. Zhang, X.-M. Zhang
School of Chemistry & Material Science
Shanxi Normal University
Taiyuan 030006, P. R. China
E-mail: zhangxm@sxnu.edu.cn

X.-M. Zhang
College of Chemistry
Taiyuan University of Technology
Taiyuan 030024, P. R. China

 The ORCID identification number(s) for the author(s) of this article can be found under <https://doi.org/10.1002/advs.202400377>

© 2024 The Authors. Advanced Science published by Wiley-VCH GmbH. This is an open access article under the terms of the [Creative Commons Attribution](#) License, which permits use, distribution and reproduction in any medium, provided the original work is properly cited.

DOI: 10.1002/advs.202400377



Scheme 1. The synthesis route of $\text{Ag}_{54}\text{Cu}_{12}$ nanocluster.

On the other hand, Cu(I) alkynyl complexes have been extensively studied as key intermediates in copper-catalyzed transformations of alkynes as well as in click chemistry synthesis of 1,2,3-triazole.^[9] The widely utilized CuAAC involves generation of Cu^I-alkynyl species of various nuclearities.^[10] Reported examples include Cu_{33} and Cu_{62} ,^[11] and Cu_{20} ^[12] nanocluster.^[13] Apart from these homogeneous intermediates, there are only sporadic reports on heterometallic intermediates involving the click reaction. However, understanding of interaction of Cu(I) and hetero-metals in heterogeneous CuAAC catalytic systems is not well clear. Recently, Zhu et al captured three crucial $\text{Au}_4\text{Cu}_4-\pi$ -alkyne intermediates and discussed an abnormal mechanism in CuAAC reaction, which is different from comproportionation reaction to dehydrogenate.^[14] Therefore, the revealing of Cu(I) and Ag(I) interaction in heterometallic Cu/Ag clusters is of significance in click chemistry of CuAAC reaction. It is still an open question whether heterometallic intermediates can be achieved by comproportionation reaction and alkyne precursor. Inspired by the widely used methodology for Cu-ethyne nanoclusters, we would like to explore the similar story in Ag-ethyne cousins.

In order to generate new heterometallic nanoclusters and intermediates in CuAAC reaction, a series of Ag-Cu-alkyne products in the system need to be obtained by alkyne ligands. Our strategy is to creatively use silver-phenylacetylene precursor instead of alkyne or copper-alkyne ligand during CuAAC reaction without azides. Silver-phenylacetylene precursor provides alkyne source for CuAAC intermediate because alkynyl as a π -acid ligand can bind to d¹⁰ ions of Au, Ag, Cu via σ - π modes and form various metal-carbon interactions.^[15] As such, the pronounced interactions of alkynyl in a variety of coordination modes may affect the physicochemical properties of metal clusters due to metal atom kernel and metal-alkyne interactions.^[16] This allows the atomic-level understanding of structure-property correlations, which in turn favours the targeted preparation of metal nanoclusters.^[17] In addition, the slow release of Ag⁺ from silver-phenylacetylene in a weakly reducing DMF can bind Cu⁺ in situ.^[18] As in Scheme 1, we envisage that the polymolybdate anion template will target Ag and Cu metal centres to aggregate in a core-shell structure, resulting in the formation of Ag-Cu clusters.

Herein, we present a 66-nuclear all-alkynyl protected peanut-shaped silver(I)/copper(I) heterometallic nanocluster, $[(\text{Mo}_4\text{O}_{16})_2@(\text{Cu}_{12}\text{Ag}_{54}(\text{PhC}\equiv\text{C})_{50})]$ ($\text{Ag}_{54}\text{Cu}_{12}$), which was synthesized by using silver-alkyne complex and protective alkyne ligands in the presence of molybdate. The two tetramolybdates $[\text{Mo}_4\text{O}_{16}]^{8-}$ mutually twisted ca. 24° were encapsulated by $\text{Cu}_{12}\text{Ag}_{54}$ cage to form a core-shell peanut-shaped $(\text{Mo}_4\text{O}_{16})_2@(\text{Cu}_{12}\text{Ag}_{54})$ nanocluster. The surface $\text{PhC}\equiv\text{C}^-$ ligands are ligated Ag and Cu in five types coordination modes to stabilize the nanocluster. The structure and composition of $\text{Ag}_{54}\text{Cu}_{12}$ were determined by high-resolution electrospray ionization mass spectrometry (ESI-TOF-MS), X-ray diffraction (XRD), energy-dispersive X-ray spectroscopy (EDS), Fourier-transform infrared (FT-IR) spectroscopy, and X-ray photoelectron spectroscopy (XPS). Furthermore, a solid-state UV-vis absorption spectrum of $\text{Ag}_{54}\text{Cu}_{12}$ showed a narrow-bandgap semiconductor with a good photocurrent response. $\text{Ag}_{54}\text{Cu}_{12}$ itself and $\text{Ag}_{54}\text{Cu}_{12}$ loaded with activated carbon as catalysts were applied in [3+2] cycloaddition reactions between alkynes and azides at ambient conditions.

2. Results and Discussion

Single X-ray diffraction analysis indicated $\text{Ag}_{54}\text{Cu}_{12}$ nanocluster crystallized in triclinic *P1* space group.^[19] The asymmetry unit contains a whole $\text{Ag}_{54}\text{Cu}_{12}$ cluster (Figure 1a). The shape of the 66-nucleus cluster resembles a peanut with $\text{Cu}_{12}\text{Ag}_{54}$ ellipsoidal cage as peanut shell and two $\text{Mo}_4\text{O}_{16}^{8-}$ groups as peanut seeds (Figure 1b). Notably, the nuclearity of $\text{Ag}_{54}\text{Cu}_{12}$ is comparable with those of the previously reported monovalent Ag-Cu heterometallic nanocluster, namely $[\text{Ag}_{74-x}\text{Cu}_x\text{O}_{12}(\text{PhC}\equiv\text{C})_{50}]_{127}$ ^[18a] and $[\text{Ag}_{40.13}\text{Cu}_{13.87}\text{S}_{19}(\text{tBuS})_{20}(\text{tBuSO}_3)_{12}]$.^[20] The overall structure contains 54 Ag atoms, 12 Cu atoms, 50 $\text{PhC}\equiv\text{C}^-$ ligands, and two Mo_4O_{16} units (Figure 1a). The $\text{Cu}_{12}\text{Ag}_{54}$ cage consists of an Ag shell on the periphery and Cu embedded in the inner shell, which generates Ag-Cu heterometallic interactions (Figure 1c,d). The shell of peanut-shaped $\text{Cu}_{12}\text{Ag}_{54}$ consists of silver triangles and tetragons with short Ag...Ag interactions of 2.84–3.41 Å (Figure 1e), whose surface is covered by 50 $\text{PhC}\equiv\text{C}^-$ groups in $\mu_3-\eta^1:\eta^1:\eta^1$, $\mu_3-\eta^1:\eta^1:\eta^2$, $\mu_3-\eta^1:\eta^2:\eta^2$, and $\mu_3-\eta^2:\eta^2:\eta^2$ coordination modes with Ag-C distances of 2.01(2)–2.704(16) Å and Cu-C

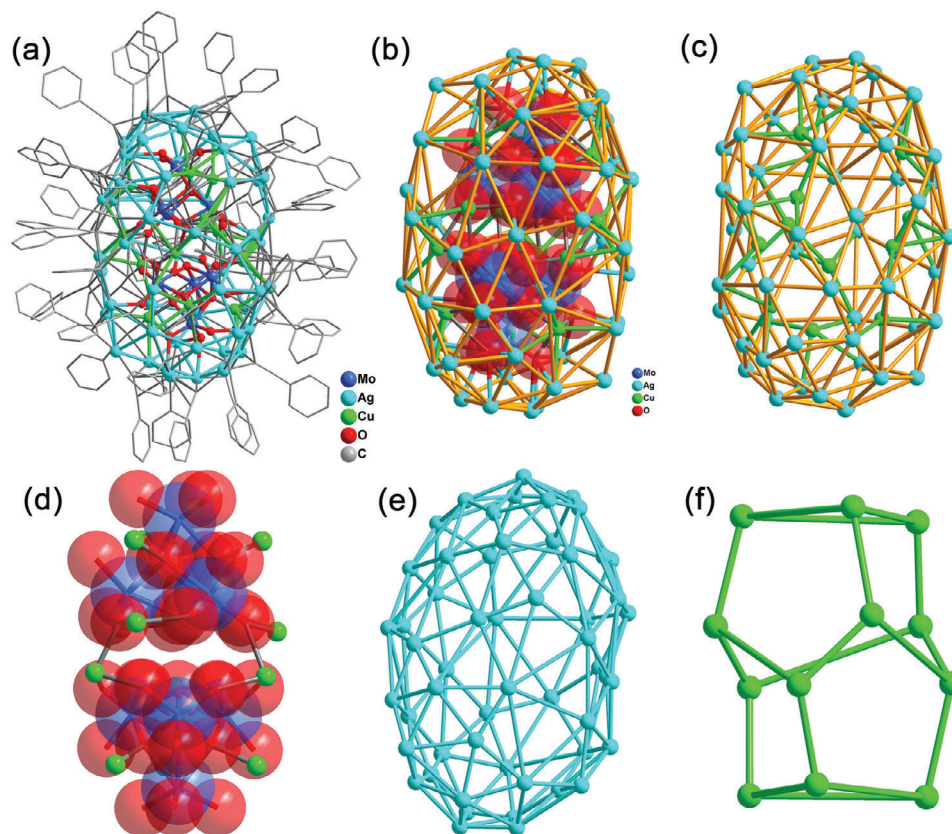


Figure 1. a) Full structure of $\text{Ag}_{54}\text{Cu}_{12}$ nanocluster. b) The core-shell peanut shaped of $\text{Ag}_{54}\text{Cu}_{12}$. c) The $\text{Cu}_{12}\text{Ag}_{54}$ ellipsoid cage as peanut shell. d) The two tetramolybdates serve as seeds for the nanocluster. e) Ag_{54} shell. f) Cu_{12} motif.

distances of 1.815(18)–1.888(13) Å. Inner wall twelve Cu atoms coordinate to carbon atoms of $\text{PhC}\equiv\text{C}^-$ and oxygen atoms of $\text{Mo}_4\text{O}_{16}^{8-}$ group, which are interacted with Ag atoms of shell with short $\text{Cu}\cdots\text{Ag}$ distances of 2.734(3)–3.056(3). Considering the arrangement of copper atoms, twelve Cu atoms form a Cu_{12} motif comprised of pentagons and triangles (Figure 1f). The 3D

packing modes of $\text{Ag}_{54}\text{Cu}_{12}$ nanoclusters in *b* and *c* directions are shown in Figure S1 (Supporting Information).

The peanut kernel consists of two independent $\text{Mo}_4\text{O}_{16}^{8-}$ tetramolybdates as seeds (Figure S3a,b, Supporting Information), which show similar cubane-like structures with T_d symmetry, with Mo–O bond distances ranging from 1.705(10) to 2.288(19) Å.^[21] The bond valence for Mo ions by valence sum (BVS) calculations (Table S2, Supporting Information) demonstrated +6. The $[\text{Mo}_4\text{O}_{16}]^{8-}$ anion was self-assembled in situ from molybdate during the solvothermal process. Surprisingly, in contrast to the orientation of $\text{Mo}_4\text{O}_{16}^{8-}$ groups in our recently reported $[\text{Cu}_3\text{Mo}_8\text{O}_{32}]^{10-}$,^[22] the two $\text{Mo}_4\text{O}_{16}^{8-}$ groups in $\text{Ag}_{54}\text{Cu}_{12}$ are not overlapped but staggered by ≈ 24 degrees (Figure S3c, Supporting Information).

Compared to reported metal nanoclusters encapsulating multiple polyoxometallates (POMs), the twisted configuration of two unconnected $[\text{Mo}_4\text{O}_{16}]^{8-}$ units is unique (reports listing these high nuclear clusters are in Table S3, Supporting Information). The unconnected arrangement of two POMs allows more oxygen sites to be exposed, which is beneficial for enhancing the template effect. Careful check revealed that two $[\text{Mo}_4\text{O}_{16}]^{8-}$ units are bonded to 12 Cu atoms through 6 μ_2 -O and 24 terminal oxygen atoms via weak $\text{Cu}\cdots\text{O}$ bonds, and to 34 Ag atoms via 20 terminal oxygen atoms. The 20 Ag atoms uncoordinated to POMs were found to be embedded into Ag_{54} shell by Ag–Cu, Ag–C,

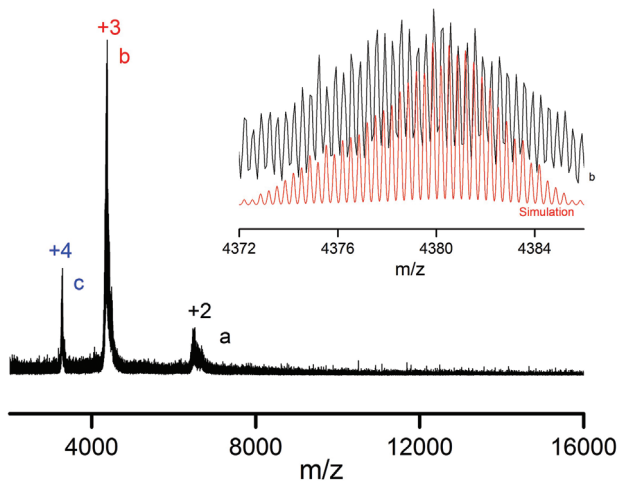


Figure 2. ESI-TOF-MS spectra of $\text{Ag}_{54}\text{Cu}_{12}$.

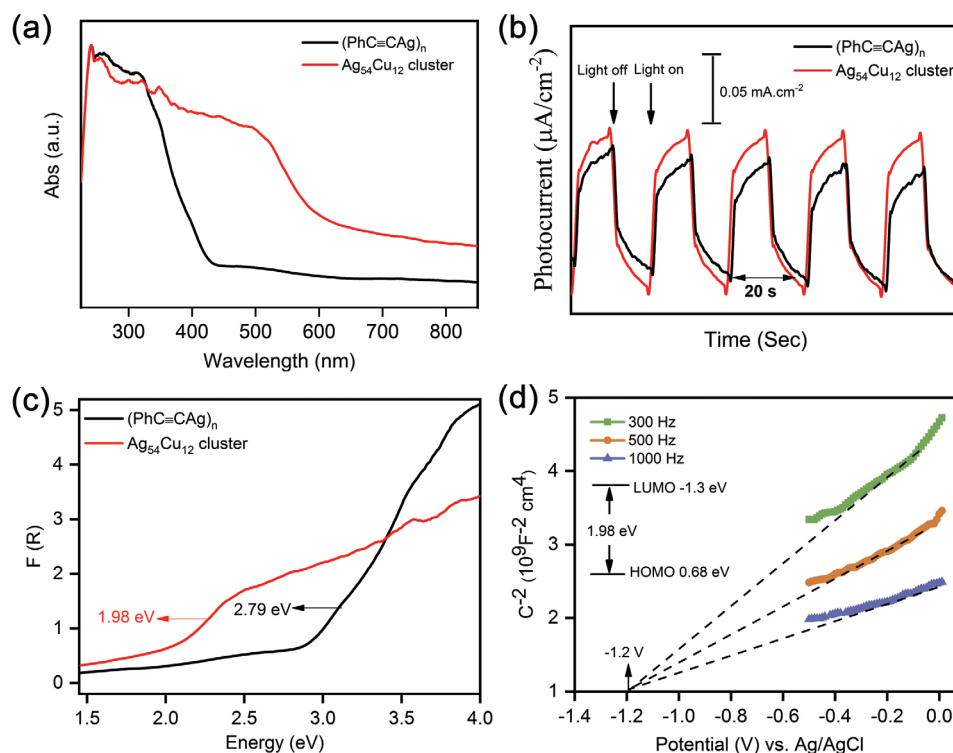


Figure 3. a) Solid-state UV–vis absorption spectra and b) photocurrent responses under UV irradiation of $(\text{PhC}\equiv\text{C}\text{Ag})_n$ and $\text{Ag}_{54}\text{Cu}_{12}$. c) Kubelka-Munk function versus energy (eV) and Tauc plots of $(\text{PhC}\equiv\text{C}\text{Ag})_n$ and $\text{Ag}_{54}\text{Cu}_{12}$. d) Mott-Schottky plot of $\text{Ag}_{54}\text{Cu}_{12}$ in a 0.2 M Na_2SO_4 aqueous solution.

and Ag–Ag interactions. The $\text{Cu}_{12}\text{Ag}_{54}$ shell was further consolidated by all alkyne ligands.

To investigate the solution behavior and composition, $\text{Ag}_{54}\text{Cu}_{12}$ cluster was monitored utilizing electrospray ionization-time of flight-mass spectrometry (ESI-TOF-MS) in the mass-to-charge ratio (m/z) range of 1000–20000. As shown in Figure 2, $\text{Ag}_{54}\text{Cu}_{12}$ was dissolved in a mixed solvent of methanol and dichloromethane. In positive ion mode, peaks with two valence states were observed in the m/z ranges of 3400–3500 and 4200–4400, respectively. The main peak b3 at the highest abundance $m/z = 4379.85$ can be attributed to $[(\text{Mo}_4\text{O}_{16})_2@(\text{Cu}_{12}\text{Ag}_{54}(\text{PhC}\equiv\text{C})_{50}(\text{CH}_3\text{OH})(\text{CH}_3\text{OH}_2)_3)]^{3+}$ (*cal.* 4379.91), which was considered to be the $\text{Ag}_{54}\text{Cu}_{12}$ molecular ion peak with three protonated MeOH molecules.

The composition of hetero-metal cluster was supported by PXRD and FI-IR spectra (Figures S4 and S5, Supporting Information, Experimental Section). XPS spectra shown the presence of Ag, Cu, Mo, C, and O elements, which was consistent with the results of EDS-mapping (Figures S6 and S7a, Supporting Information). High-resolution spectra clearly illustrated the valences of metal ions of $\text{Ag}_{54}\text{Cu}_{12}$. As shown in Figure S7b (Supporting Information), XPS data of the Ag $3d_{5/2}$ and Ag $3d_{3/2}$ binding energies are 368.26 and 374.24 eV, respectively, confirming that Ag atoms in the cluster are positively charged.^[23] The Mo binding energy at 232.9 and 235.2 eV in Figure S7c (Supporting Information) can be attributed to Mo^{6+} $3d_{5/2}$ and $3d_{3/2}$ spin-splitting slits.^[24] Figure S7d (Supporting Information) shows XPS peaks of monovalent Cu(I). The Cu LMM Auger chemical shift also

showed monovalent Cu^I state (Figure S9, Supporting Information).

The solid-state UV absorption spectra of $\text{Ag}_{54}\text{Cu}_{12}$ show a broadband absorption in the wavelength range 300–400 nm, which is attributed to the $\pi \rightarrow \pi^*$ transition due to appearance of similar band in $(\text{PhC}\equiv\text{C}\text{Ag})_n$ precursor. The optical bandgap of $\text{Ag}_{54}\text{Cu}_{12}$ was determined by Tauc equation to be 1.98 eV, which is narrower than that of 2.79 eV in precursor $(\text{PhC}\equiv\text{C}\text{Ag})_n$ (Figure 3c). This suggests that $\text{Ag}_{54}\text{Cu}_{12}$ has potential as a narrow-band-gap semiconductor.^[18a,25] The photoelectrochemical behavior of $\text{Ag}_{54}\text{Cu}_{12}$ was tested in a typical three-electrode system in a 0.2 M Na_2SO_4 aqueous solution. Compared with $(\text{PhC}\equiv\text{C}\text{Ag})_n$, an obvious photocurrent response was detected upon on-off cycling irradiation, indicating a better electron and hole separation efficiency of $\text{Ag}_{54}\text{Cu}_{12}$. The photocurrent density could reach up to $0.11 \mu\text{A cm}^{-2}$, which remained nearly constant with increased test times, indicating high photophysical stability of $\text{Ag}_{54}\text{Cu}_{12}$. Considering the broad absorption semiconductor property of $\text{Ag}_{54}\text{Cu}_{12}$, Mott-Schottky (M-S) measurements were performed at frequencies of 300, 500 and 1000 Hz in darkness (Figure 3d). The positive slope of the C^{-2} -E plot confirms that $\text{Ag}_{54}\text{Cu}_{12}$ is an *n*-type semiconductor.^[26] The flat band potential (EFB) was determined by the intersection to be ≈ -1.3 V versus Ag/AgCl, corresponding to a potential of -0.68 V versus NHE. It is expected that Based on the previous reports, the conduction band edge of semiconductor should be ≈ 0.10 V more negative than the EFB. Therefore, it can be estimated that the conduction band (LUMO) of $\text{Ag}_{54}\text{Cu}_{12}$ is approximately -1.2 V versus NHE.

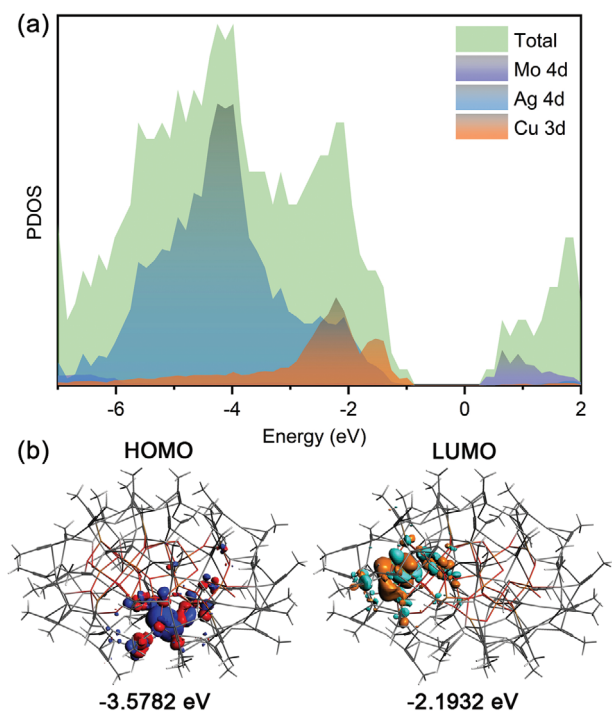


Figure 4. a) Total and partial DOS of $\text{Ag}_{54}\text{Cu}_{12}$ cluster. b) Frontier molecular orbitals: HOMO and LUMO.

The valence band (HOMO) of $\text{Ag}_{54}\text{Cu}_{12}$ is estimated to be 0.68 V versus NHE.

To understand the role of electron orbitals around the Fermi level, the total and partial densities of states (DOSs) of $\text{Ag}_{54}\text{Cu}_{12}$ were calculated. As is shown **Figure 4a**, the top of the valence

band is mainly composed of metal Ag 4d, Cu 3d, and a few Mo 4d states. The bottom of the conduction band is dominated by metal Mo 4d, a few Ag 4d and Cu 3d, proving that the optical properties of $\text{Ag}_{54}\text{Cu}_{12}$ are determined by Ag, Cu and $[\text{Mo}_4\text{O}_{16}]^{8-}$ anion template. The HOMO-LUMO bandgap difference is calculated to be 1.383 eV, in well agreement the experimental value. The lowest empty orbital of $\text{Ag}_{54}\text{Cu}_{12}$ is primarily located in the Mo 4d orbital on $[\text{Mo}_4\text{O}_{16}]^{8-}$, while the highest occupied orbital is mainly concentrated in the Mo 4d and C 2p of $\text{Ph}\equiv\text{C}^-$ (**Figure 4b**). This indicates that $[\text{Mo}_4\text{O}_{16}]^{8-}$ anion has a significant effect on the optical properties of $\text{Ag}_{54}\text{Cu}_{12}$. Several high lying occupied orbitals, such as HOMO-1, HOMO-2, HOMO-3, and HOMO-4, are almost entirely contributed by orbitals of peripheral ligand $\text{C}\equiv\text{C}$ bonds (**Figure S9**, Supporting Information). According to Frontier molecular orbitals theory, LUMO is logically considered electrophilic, which may partly explain the fact that the outer O atoms of the non-coordinated/exposed portion of $\text{Mo}_4\text{O}_{16}^{8-}$ unit are less likely to further coordinate with the Ag atoms.

Copper-catalyzed [3+2] Huisgen cycloadditions of terminal alkynes and organic azides (CuAAC) were the cornerstone of Meldal and Sharpless research, most of which involved homometallic Cu-based materials.^[27,28] To investigate and develop heterometallic 1,3-dipole cycloaddition reaction catalysis, $\text{Ag}_{54}\text{Cu}_{12}$ was implemented by using phenylacetylene and benzyl azide at 40 °C as the model reaction. This reaction exhibits completely regioselectivity and is a powerful method for the rapid assembly of 1,4-disubstituted-1,2,3-triazoles. The solution of $\text{Ag}_{54}\text{Cu}_{12}$ cluster was gradually added to a suspension of activated carbon/titanium dioxide in ethanol, and resulted mixture was stirred and centrifuged to give C/ TiO_2 supported nanocluster catalysts. Transmission electron microscopy (TEM) illustrated that all particles of as-synthesized products were less than 2 nm

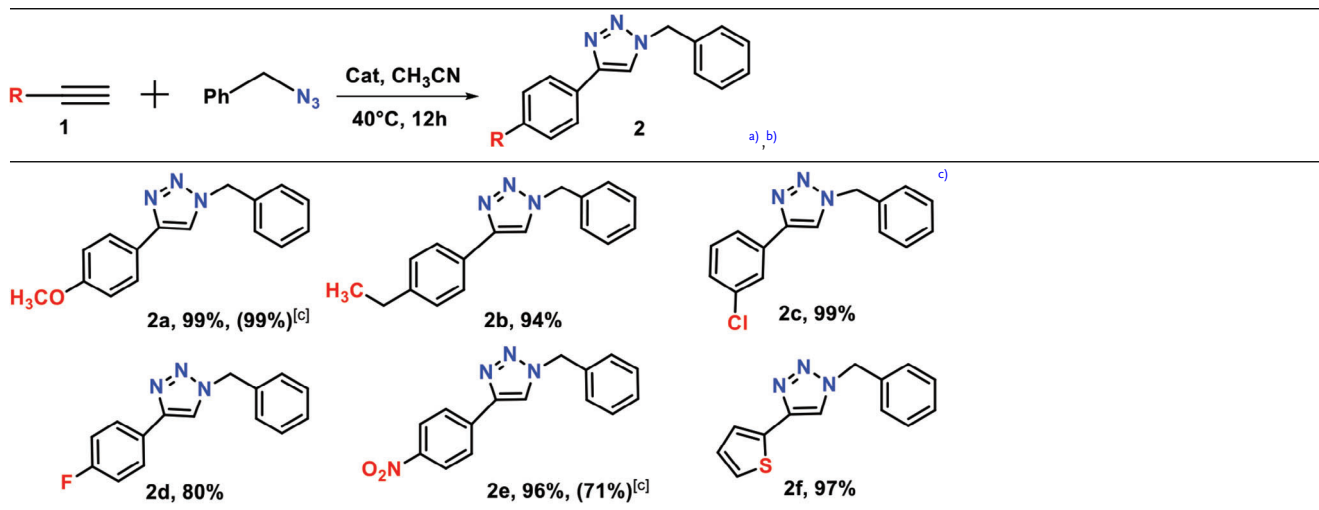
Table 1. Cycloaddition of phenylacetylene and benzyl azide.

Entry ^{a)}	Catalyst	Cu Loading [mmol, %] ^{b)}	Solvent	Time	Yield [%] ^{c)}	TOF
1	$\text{Ag}_{54}\text{Cu}_{12}/\text{C}$	0.23	CH_3CN	12 h	80%	28.98
2	$\text{Ag}_{54}\text{Cu}_{12}/\text{C}$	0.46	CH_3CN	12 h	99%	17.93
3	$\text{Ag}_{54}\text{Cu}_{12}/\text{C}$	0.23	CH_3OH	12 h	45%	16.30
4	$\text{Ag}_{54}\text{Cu}_{12}/\text{TiO}_2$	0.23	CH_3CN	12 h	13%	4.71
5	$\text{Ag}_{54}\text{Cu}_{12}/\text{TiO}_2$	0.46	CH_3CN	12 h	70%	12.68
6	$\text{Ag}_{54}\text{Cu}_{12}$	2.3	CH_3CN	12 h	88%	3.19
7	C	—	CH_3CN	24 h	0	—
8	TiO_2	—	CH_3CN	24 h	0	—
9	AgSO_3CF_3	—	CH_3CN	24 h	0	—
10	Na_2MoO_4	—	CH_3CN	24 h	0	—
11	None	—	CH_3CN	24 h	0	—

^{a)} Reaction conditions: phenylacetylene (0.22 mmol), benzyl azide (0.2 mmol), acetonitrile (1 mL), 40 °C. ^{b)} Catalyst loading defined as mmol% Cu-based $\text{Ag}_{54}\text{Cu}_{12}$ cluster.

^{c)} Isolated yield.

Table 2. Scope of benzyl azide with different alkynes.



^{a)} Reaction conditions: phenylacetylene (0.22 mmol), benzyl azide (0.2 mmol), acetonitrile (1 mL), Ag₅₄Cu₁₂/C (Cu loading 0.46% mmol), 40 °C. ^{b)} Isolated yield. ^{c)} Reaction conditions: phenylacetylene (0.22 mmol), benzyl azide (0.2 mmol), acetonitrile (1 mL), Ag₅₄Cu₁₂ (Cu loading 2.3% mmol), 40 °C.

in size, indicating good dispersion of the clusters loaded on the activated carbon (Figure S11, Supporting Information).

First, the influence of different solvents on the reaction was investigated. A relatively higher yield was realized in CH₃CN (99%), compared to CH₃OH solvent (Table 1, entries 1–5). In addition, the effect of supports and loading capacity was also investigated under the same reaction conditions, and a high isolated yield of 99% was realized (Table 1, entry 1–2 and 4–5). The unsupported Ag₅₄Cu₁₂ NCs gave a lower isolated yield of 88% (Table 1, entry 6). Importantly, the control experiments showed that Ag₅₄Cu₁₂ significantly contributes to the cycloaddition process (Table 1, entries 7–11).

Based on optimized standard conditions, the generality of cycloaddition was explored for various aryl-terminated acetylenes and the corresponding results were summarized in Table 2. Good yields (90%–94%) were obtained for substituted aryl alkynes with both electron-donating (–OCH₃ and –CH₃) and electron-withdrawing (–F, –Cl, and –NO₂) substituents (Table 2, entries 1–6). These results demonstrated the important interaction between Ag₅₄Cu₁₂ and activated carbon substrate.

Interestingly, some 1,2,3-triazole products were crystallized from reaction environment (Tables 1, entry 6 and 2, entries 7–8). The single crystal data of products were collected and solved (Figure S12a and Tables S5 and S6, Supporting Information), directly confirming their corresponding identity. Both Ag₅₄Cu₁₂ and Ag₅₄Cu₁₂/C as catalysts exhibited excellent cycle stability after six experiments (Figure S12b, Supporting Information). These results demonstrated that Ag₅₄Cu₁₂ NCs could be a high-performance molecular catalysts for CuAAC.

3. Conclusion

In conclusion, we have isolated an all-alkyne protected silver(I)/copper(I) heterometallic nanocluster, [(Mo₄O₁₆)₂@Cu₁₂Ag₅₄(PhC≡C)₅₀] (Ag₅₄Cu₁₂), which was synthesized by the reduction of Cu (II) salt and copper powder in

presence with (PhC≡CAg)_n and Na₂MoO₄ under solvothermal method. Two mutually twisted [Mo₄O₁₆]^{8–} anions were encapsulated by Cu₁₂Ag₅₄ cage to form a core-shell peanut-shaped (Mo₄O₁₆)₂@Cu₁₂Ag₅₄ nanocluster. The surface PhC≡C[–] ligands are ligated to Ag and Cu in σ-π modes to stabilize the nanocluster. XRD, XPS, and ESI-TOF-MS certify the structure and composition of Ag₅₄Cu₁₂. The *n*-type narrow-band-gap material was confirmed by solid state UV-vis spectra and DFT calculation. Furthermore, Ag₅₄Cu₁₂ itself and Ag₅₄Cu₁₂/C are good catalysts for 1,3-dipole cycloaddition between alkynes and azides at ambient conditions. Different from conventional methods for heterometallic clusters, the comproportionation reaction in the work could provide an effective method in controlling reduction of double metal salts and formation of heteroatomic high-nuclearity monovalent copper alkynyl clusters.

Supporting Information

Supporting Information is available from the Wiley Online Library or from the author.

Acknowledgements

This work was financially supported by the Natural Science Foundation of China (91961201).

Conflict of Interest

The authors declare no conflict of interest.

Data Availability Statement

The data that support the findings of this study are available from the corresponding author upon reasonable request.

Keywords

1,3-dipole cycloadditions, CuAAC reaction, Heterometallic nanoclusters, Intermediate

Received: January 10, 2024

Revised: March 1, 2024

Published online: April 1, 2024

- [1] a) M.-M. Zhang, X.-Y. Dong, Y.-J. Wang, S.-Q. Zang, T. C. W. Mak, *Coord. Chem. Rev.* **2022**, *453*, 214315; b) S. Sharma, K. K. Chakrahari, J. Y. Saillard, C. W. Liu, *Acc. Chem. Res.* **2018**, *51*, 2475; c) T. Kawawaki, Y. Imai, D. Suzuki, S. Kato, I. Kobayashi, T. Suzuki, R. Kaneko, S. Hossain, Y. Negishi, *Chem.-Eur. J.* **2020**, *26*, 16150; d) X.-H. Ma, Y. Si, L.-L. Luo, Z.-Y. Wang, S.-Q. Zang, T. C. W. Mak, *ACS Nano* **2022**, *16*, 5507; e) S. Hossain, Y. Niihori, L. V. Nair, B. Kumar, W. Kurashige, Y. Negishi, *Acc. Chem. Res.* **2018**, *51*, 3114.
- [2] a) J. Chai, Y. Lv, S. Yang, Y. Song, X. Zan, Q. Li, H. Yu, M. Wu, M. Zhu, *J. Phys. Chem. C* **2017**, *121*, 21665; b) S. Wang, Y. Song, S. Jin, X. Liu, J. Zhang, Y. Pei, X. Meng, M. Chen, P. Li, M. Zhu, *J. Am. Chem. Soc.* **2015**, *137*, 4018.
- [3] a) X. Zou, Y. Li, S. Jin, X. Kang, X. Wei, S. Wang, X. Meng, M. Zhu, *J. Phys. Chem. Lett.* **2020**, *11*, 2272; b) J. Yang, R. Pang, D. Song, M.-B. Li, *Nanoscale Adv.* **2021**, *3*, 2411.
- [4] a) S. Wang, Q. Li, X. Kang, M. Zhu, *Acc. Chem. Res.* **2018**, *51*, 2784; b) Y. Negishi, T. Iwai, M. Ide, *Chem. Commun.* **2010**, *46*, 4713; c) S. Takano, S. Ito, T. Tsukuda, *J. Am. Chem. Soc.* **2019**, *141*, 15994.
- [5] R. Anumula, P. Xiao, C. Cui, H. Wu, G. Cui, W.-H. Fang, Z. Luo, J. Yao, *Nanoscale* **2020**, *12*, 7864.
- [6] a) H.-Y. Zhuo, H.-F. Su, Z.-Z. Cao, W. Liu, S.-A. Wang, L. Feng, G.-L. Zhuang, S.-C. Lin, M. Kurmoo, C.-H. Tung, D. Sun, L.-S. Zheng, *Chem.-Eur. J.* **2016**, *22*, 17619; b) L. L.-M. Zhang, T. C. W. Mak, *Angew. Chem., Int. Ed.* **2017**, *56*, 16228.
- [7] a) Z. Gan, N. Xia, Z. Wu, *Acc. Chem. Res.* **2018**, *51*, 2774; b) X. Liu, D. Astruc, *Adv. Mater.* **2017**, *29*, 1605305; c) B.-L. Han, Z. Wang, R. K. Gupta, L. Feng, S. Wang, M. Kurmoo, Z.-Y. Gao, S. Schein, C.-H. Tung, D. Sun, *ACS Nano* **2021**, *15*, 8733.
- [8] a) M. Zhu, P. Wang, N. Yan, X. Chai, L. He, Y. Zhao, N. Xia, C. Yao, J. Li, H. Deng, Y. Zhu, Y. Pei, Z. Wu, *Angew. Chem., Int. Ed.* **2018**, *57*, 4500; b) A. G. M. da Silva, T. S. Rodrigues, S. J. Haigh, P. H. C. Camargo, *Chem. Commun.* **2017**, *53*, 7135; c) M.-B. Li, S.-K. Tian, Z. Wu, R. Jin, *Chem. Commun.* **2015**, *51*, 4433.
- [9] a) L. Liang, D. Astruc, *Coord. Chem. Rev.* **2011**, *255*, 2933; b) B. T. Worrell, J. A. Malik, V. V. Fokin, *Science* **2013**, *340*, 457; c) B. R. Buckley, S. E. Dann, D. P. Harris, H. Heaney, E. C. Stubbs, *Chem. Commun.* **2010**, *46*, 2274; d) R. Singh, G. Singh, N. George, G. Singh, A. Devi, H. Singh, G. Kaur, J. Singh, *RSC Adv.* **2023**, *13*, 32399; e) G. Singh, R. Singh, N. George, G. Singh, G. K. Sushma, G. Kaur, H. Singh, J. Singh, *J. Photochem. Photobiol. A* **2023**, *441*, 114741; f) N. George, G. Singh, R. Singh, G. Singh, H. S. Priyanka, G. Kaur, J. Singh, *J. Mol. Struct.* **2023**, *1288*, 135666.
- [10] a) J. E. Hein, V. V. Fokin, *Chem. Soc. Rev.* **2010**, *39*, 1302; b) V. K. Tiwari, B. B. Mishra, K. B. Mishra, N. Mishra, A. S. Singh, X. Chen, *Chem. Rev.* **2016**, *116*, 3086.
- [11] L. M. Zhang, T. C. Mak, *J. Am. Chem. Soc.* **2016**, *138*, 2909.
- [12] A. W. Cook, Z. R. Jones, G. Wu, S. L. Scott, T. W. Hayton, *J. Am. Chem. Soc.* **2018**, *140*, 394.
- [13] a) R. Buschbeck, P. J. Low, H. Lang, *Coord. Chem. Rev.* **2011**, *255*, 241; b) H. Lang, A. Jakob, B. Milde, *Organometallics* **2012**, *31*, 7661; c) D. M. P. Mingos, R. Vilar, D. Rais, *J. Organomet. Chem.* **2002**, *641*, 126.
- [14] Y. Fang, K. Bao, P. Zhang, H. Sheng, Y. Yun, S. X. Hu, D. Astruc, M. Zhu, *J. Am. Chem. Soc.* **2021**, *143*, 1768.
- [15] X.-K. Wan, S.-F. Yuan, Q. Tang, D.-E. Jiang, Q.-M. Wang, *Angew. Chem.* **2015**, *127*, 6075.
- [16] T. U. Connell, S. Sandanayake, G. N. Khairallah, J. M. White, R. A. J. O'Hair, P. S. Donnelly, S. J. Williams, *Dalton Trans.* **2013**, *42*, 4903.
- [17] X. Wei, K. Chu, J. R. Adsetts, H. Li, X. Kang, Z. Ding, M. Zhu, *J. Am. Chem. Soc.* **2022**, *144*, 20421.
- [18] a) Y. Yang, T. Jia, Y.-Z. Han, Z.-A. Nan, S.-F. Yuan, F.-L. Yang, D. Sun, *Angew. Chem., Int. Ed.* **2019**, *58*, 12280; b) Z. Wang, R. K. Gupta, G.-G. Luo, D. Sun, *Chem. Rec.* **2020**, *20*, 389; c) Y.-M. Su, B.-Q. Ji, Z. Wang, S.-S. Zhang, L. Feng, Z.-Y. Gao, Y.-W. Li, C.-H. Tung, D. Sun, L.-S. Zheng, *Sci. China Chem.* **2021**, *64*, 1482.
- [19] Deposition numbers 2243094 contain the supplementary crystallographic data for this paper. These data are provided free of charge by the joint Cambridge Crystallographic Data Centre and Fachinformationszentrum Karlsruhe Access Structures service.
- [20] S. Yang, J. Chai, H. Chong, Y. Song, H. Yu, M. Zhu, *Chem. Commun.* **2018**, *54*, 4314.
- [21] M. M. Borel, J. Chardon, A. Leclaire, A. Grandin, B. Raveau, *J. Solid State Chem.* **1994**, *112*, 317.
- [22] J.-P. Gao, Z. Qi, F.-Q. Zhang, X.-M. Zhang, *Nanoscale* **2022**, *14*, 4469.
- [23] a) R.-W. Huang, Q.-Q. Xu, H.-L. Lu, X.-K. Guo, S.-Q. Zang, G.-G. Gao, M.-S. Tang, T. C. W. Mak, *Nanoscale* **2015**, *7*, 7151; b) W.-Q. Shi, Z.-J. Guan, J.-J. Li, X.-S. Han, Q.-M. Wang, *Chem. Sci.* **2022**, *13*, 5148.
- [24] L. Lin, Z. K. Yang, Y.-F. Jiang, A.-W. Xu, *ACS Catal.* **2016**, *6*, 4449.
- [25] X.-K. Wan, W. W. Xu, S.-F. Yuan, Y. Gao, X.-C. Zeng, Q.-M. Wang, *Angew. Chem. Int. Ed.* **2015**, *54*, 9683.
- [26] a) Z. Wang, L. Li, L. Feng, Z.-Y. Gao, C.-H. Tung, L.-S. Zheng, D. Sun, *Angew. Chem. Int. Ed.* **2022**, *61*, 202200823; b) S. Saha, G. Das, J. Thote, R. Banerjee, *J. Am. Chem. Soc.* **2014**, *136*, 14845.
- [27] a) C. W. Tornøe, C. Christensen, M. Meldal, *J. Org. Chem.* **2002**, *67*, 3057; b) V. V. Rostovtsev, L. G. Green, V. V. Fokin, K. B. Sharpless, *Angew. Chem., Int. Ed.* **2002**, *41*, 2596.
- [28] a) M. Meldal, C. W. Tornøe, *Chem. Rev.* **2008**, *108*, 2952; b) Z. E. Blastik, S. Voltrová, V. Matoušek, B. Jurásek, D. W. Manley, B. Klepetářová, P. Beier, *Angew. Chem. Int. Ed.* **2017**, *56*, 346.